High-pressure protein crystallography (HPPX): instrumentation, methodology and results on lysozyme crystals

R. Fourme,[a]* R. Kahn,[c] M. Mezouar,[d] E. Girard,[c] C. Hoerentrup,[a] T. Prangé[a,b] and I. Ascone[a]

[a]LURE, UMR 130 CNRS-CEA-MRT, Bâtiment 209D, Université Paris-Sud, F91898 Orsay CEDEX, France, [b]Laboratoire de Cristallographie et RMN Biologiques, UMR 8015 CNRS, Faculté de Pharmacie, 4 Avenue de l'Observatoire, F75006 Paris, France, [c]IBS, 41 Rue Jules Horowitz, F38027 Grenoble CEDEX, France, and [d]ESRF, BP 220, F38027 Grenoble CEDEX, France. E-mail: roger.fourme@lure.u-psud.fr

A new set-up and associated methodology for the collection of angle-dispersive diffraction data from protein crystals submitted to high hydrostastic pressure have been developed on beamline ID30 at the ESRF. The instrument makes use of intense X-rays of ultra-short wavelength emitted by two collinear undulators, and combines a membrane-driven diamond-anvil cell mounted on a two-axis goniometer and an imaging-plate scanner. Sharp and clean diffraction pictures from tetragonal crystals of hen egg-white lysozyme (tHEWL) and orthorhombic crystals of bovine erythrocyte Cu, Zn superoxide dismutase (SOD) were recorded at room temperature and pressures up to 0.915 and 1.00 GPa, respectively. The compressibility of tHEWL was determined from unit-cell parameters determined at 24 different pressures up to 0.915 GPa. High-pressure diffraction data sets from several crystals of tHEWL were collected and analyzed. Merging of data recorded on different crystals at 0.30 and 0.58 GPa produced two sets of structure amplitudes with good resolution, completeness, redundancy and $R_{\rm sym}$ values. A third set at 0.69 GPa was of a similar quality except a lower completeness. The three structures have been refined. The pressure-induced loss of crystalline order in a tHEWL crystal beyond 0.82 GPa was captured through a series of diffraction pictures.

Keywords: high pressure; protein crystallography; diamond-anvil cell; lysozyme.

1. Introduction

Pressure effects are governed by Le Chatelier's principle, which states that at equilibrium a system tends to minimize the effect of any external factor that perturbs it. Consequently, an increase in pressure† favours reduction of the volume of a system. In fact, pressure permits us to isolate those effects that depend exclusively upon the volume, whereas temperature changes result in simultaneous changes in volume and thermal energy in a way that makes it difficult to separate their effects. Pressure variations have other interesting characteristics. They do not change significantly solvent properties. Pressure propagates quickly and, in the case of hydrostatic compression, perfectly uniformly. Bi-directional (increase/decrease) pressure changes are possible and the amplitude of a pressure jump can be easily and repeatedly varied, hence accumulation over several cycles is possible.

† Pressure measurements in cited articles have been converted to GPa on the basis that 1 GPa $\simeq$ 10 kbar $\simeq 10^4$ atm.

Recent decades have witnessed a growing interest in introducing pressure as a variable acting on biosystems (Mozhaev *et al.*, 1996). One of these reasons is the possibility of applying pressure in specific biotechnological areas. On the other hand, it also becomes clear that, along with such parameters as temperature and solvent conditions, pressure can be used for a more detailed thermodynamic and kinetic description of bioprocesses and biosystems and regulation of their behaviour (Gross & Jaenicke, 1994). For example, in protein denaturation studies, high hydrostatic pressure provides unique information on unfolding mechanisms (Silva & Weber, 1993; Jonas & Jonas, 1994).

Today, most methods that are routinely used at atmospheric pressure for studies of protein structure and kinetics have been adapted to high-pressure studies of biomolecules. A list of these methods with a single reference describing the application of the method under high-pressure conditions in the most comprehensive manner has been given by Mozhaev *et al.* (1996). This list includes high-pressure protein crystallography (HPPX) but these studies are scarce. The combination of the complexity of high-pressure experiments and single-crystal protein crystallography acted as a deterrent. X-ray studies of three-dimensional structures of proteins at high pressure have, to our knowledge, been performed on tetragonal hen egg-white lysozyme (tHEWL) (Kundrot & Richards, 1987), *Staphyloccocal* nuclease (Ekstrom *et al.*, 1995) and sperm whale metmyoglobin (Urayama, 1999), using a blind cylindrical beryllium cell limited to 0.2 GPa, as originally designed by Kundrot & Richards (1986). Katrusiak & Dauter (1996) used a diamond-anvil cell to perform compressibility measurements on lysozyme crystals. Another cell was described by Kriechbaum *et al.* (1994).

At the ESRF (European Synchrotron Radiation Facility, Grenoble, France) we have recently implemented HPPX on ID30, a beamline dedicated to high-pressure studies. Crystals of tHEWL and bovine erythrocyte Cu, Zn superoxide dismutase (SOD) were compressed gradually up to 0.915 and 1.00 GPa, respectively. Several high-quality diffraction data sets were collected at room temperature and analyzed for both proteins. In the present article we report results for HEWL, a monomeric protein. Results on SOD, a dimeric protein, will be published elsewhere (Ascone *et al.*, 2001).

2. Material and methods

2.1. *Instrumentation*

The schedule of conditions for HPPX is the following. A protein crystal contains from 30 to 80% by weight of solvent – the water, salts and other small molecules present in the crystallizing solution. This solvent and the liquor in which the crystal is bathed communicate through channels within the crystal structure; if the pressure variation is slow enough, both phases will remain in equilibrium, thus minimizing crystal stress. As hydrostatic compression is required, the useful domain of pressure and temperature is defined by the phase diagram of the liquor. Assuming that the liquor contains essentially water, the useful pressure domain ranges from atmospheric pressure to about 1 GPa and 2 GPa at room temperature and 350 K, respectively. When the desired pressure has been reached and data collection proceeds, the pressure should be kept reasonably constant. Therefore, the useful pressure range of a HPPX cell is from atmospheric pressure to about 2 GPa with fine pressure tunability and stability. A key feature is large optical apertures, in order to collect diffraction data over a large rotation angle, thus avoiding the use of several crystals to obtain reasonably high completeness, especially in the case of crystals with a low-symmetry space group. A system for determining the absolute value of pressure should be provided.

Optical observation should be possible at any time. Considerations that are critical for the collection of high-quality diffraction data include: data completeness, resolution and redundancy; signal-to-noise ratio of Bragg spots; detector characteristics (DQE, point spread function, readout time); and minimization and/or correction of X-ray absorption by cell components. For HPPX, a near-parallel and very intense X-ray beam of ultra-short wavelength is optimal. Ultra-short-wavelength X-rays are less absorbed by cell walls, diffraction is confined in a narrow 2θ range and the crystal-to-detector distance may be large. The decline in scattering power while decreasing wavelength is compensated by the high intensity which also allows narrow beam collimation. Finally, owing to the condition of hydrostaticity, data collection will proceed at room or moderately low temperature. In such conditions, rapid crystal degradation is foreseen, and data-collection strategy has to be designed accordingly.

We have solved most technical problems of this basic schedule by combining the use of radiation from a pair of undulators on the ID30 beamline, a diamond-anvil cell and an imaging-plate detector.

2.1.1. *X-ray source and optics*. ID30 is equipped with three collinear insertion devices (ID) on a high-β section (with a very small divergence at the cost of a slightly enlarged source), two undulators (35 and 40 mm periods) and a multipole wiggler. These IDs generate very bright beams at ultra-short X-ray wavelengths (down to about 0.25 and 0.05 Å for undulators and wiggler, respectively). These characteristics are well adapted to high-pressure experiments. Optics include a water-cooled Si(111) channel-cut monochromator and removable Kirkpatrick–Baez platinum-coated mirrors. We aimed at keeping the beam divergence as small as possible in order to obtain small diffraction spots even with the sample-to-detector distance in the range 0.6–0.8 m required for operation at ultra-short wavelengths. For this reason, we used unfocused undulator radiation. The size of the monochromatic beam was reduced by a crossed pair of tungsten slits to typically 50 µm × 50 µm.

2.1.2. *Goniometer*. The beamline incorporates a high-precision two-circle goniometer (rotations are about a vertical ω-axis and a χ-axis in the horizontal plane) installed on a stacking of three orthogonal translation tables (Fig. 1). The detector arm rotates around a third axis coaxial with the ω-axis. This goniometer can accommodate various high-pressure cells, including diamond-anvil cells. Positioning (including that of independent-jaws micrometre-size slits) and centring the sample to an accuracy better than 1 µm is standard. The goniometer is equipped with a photodiode mounted on a pneumatic actuator that sets it on or off the X-ray beam. This photodiode, located between the pressure cell and the detector, is used for the initial centring of the diamond cell (as described later) as well as for rapid check of the alignment after each compression.

2.1.3. *Diamond anvil cell (DAC)*. With respect to beryllium cells (Kundrot & Richards, 1986), DACs have extended capabilities, especially pressure range, optical observation and parasitic scattering. High pressure is generated in a cavity machined in a metal gasket (Van Valkenburg, 1962) squeezed between two diamond anvils. The cavity is filled with a liquid ensuring hydrostatic compression of the sample. We have used two identical cylindrically symmetric DACs of the cylinder–piston type (Chervin *et al.*, 1995), one cell being loaded while the other used for data collection. As in the cell designed by Fourme (1968) for single-crystal X-ray diffraction, the thrust is not generated by a lever arm but by a pneumatic device. Here, the device is an internal membrane ram (Le Toullec *et al.*, 1988), a solution that provides fine pressure-monitoring capability and good mechanical stability. Pressurization is obtained by letting He gas into the membrane chamber through a thin stainless-steel flexible tubing from an external pressure control gas source (Fig. 2). The diamond anvils had a standard Drukker shape with culet diameter $\simeq$ 600 µm and height 2.47 mm. Cells used for our experiments were not optimized for X-ray diffraction, as apertures for entrance and exit beams were only ∼42 degrees.

2.1.4. *Detector*. With respect to usual protein crystallography, the additional requirement for an area detector is high detective quantum efficiency (DQE) at ultra-short wavelengths. A large sensitive surface is also useful, as a larger crystal-to-detector distance, D, improves the signal-to-background ratio of Bragg spots on the detector. In effect, rays diffracted by a perfect crystal bathed in the near-parallel undulator beam have a very low divergence making spot size almost independent on D. In contrast, the intensity of Compton

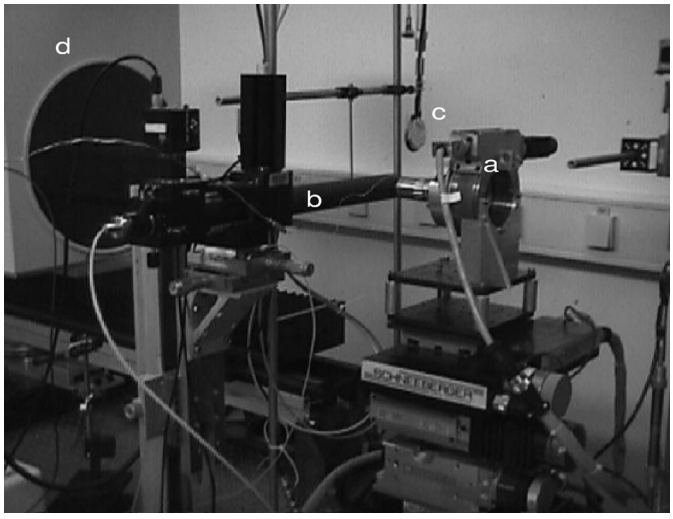

Figure 1
View of a few components of the equipment for HPPX on ID30. (*a*) Goniometer with the high-pressure cell inserted in the χ-circle. (*b*) Optical system of the on-line pressure-determination device shown here on the axis of the X-ray beam. This system is moved off the X-ray beam during data collection. (*c*) Photodiode (shown here set off the beam). (*d*) Imaging-plate scanner.

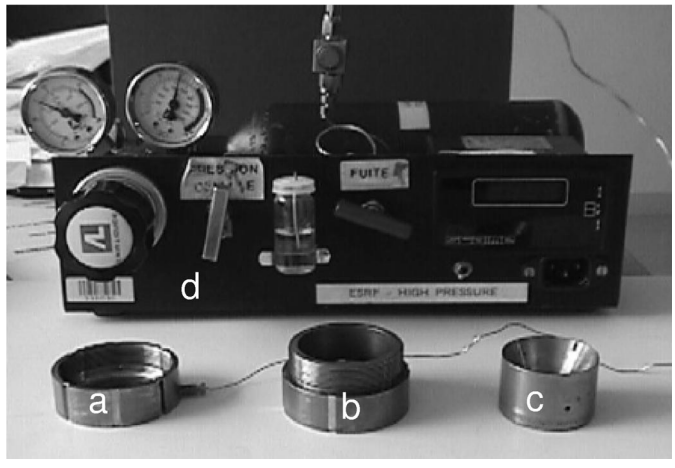

Figure 2
Components of the high-pressure cell. (*a*) Cap, with membrane chamber and gas inlet. (*b*) Body, which bears the lower diamond-anvil seat. (*c*) Piston, which bears the upper diamond-anvil seat. (*d*) External pressure control gas source, connected to the gas inlet by a 1.6 mm outer-diameter stainless-steel flexible tubing.

scattering by diamonds varies as D^{-2}. We have used a standard MAR345 imaging-plate scanner (from X-ray Research) equipped with an imaging plate (STN5 from Fuji) and mounted perpendicular to the X-ray beam. This scanner was interfaced with the goniometer through the SPEC software, allowing the rotation camera mode of data collection usual in protein crystallography. The pixel size was set to 150 μm × 150 μm. The sample-to-detector distance and the imaging-plate tilt with respect to the X-ray beam were calibrated using the powder pattern of a 30 μm-thick layer of silicon powder mounted in a replica of the diamond cells.

2.1.5. *Pressure determination*. The direct determination of the actual pressure is essential, since the relation between the gas pressure applied on the membrane and the pressure within the cavity depends on the characteristics and history of each gasket and each particular loading. This determination is performed using a classical method based on the fact that laser-excited fluorescence of ruby (R_1 line, $\lambda = 694.2$ nm at ambient pressure) is pressure-dependent (Mao *et al.*, 1978). The equipment is a commercial product (from Betsa). The fluorescence wavelength is determined with a miniature grating spectrometer calibrated in the same wavelength range using three emission lines of neon emitted by a small neon lamp. The sensitivity and the precision of the pressure determination are about 0.001 and 0.01 GPa, respectively.

ID30 is equipped with two such devices. An off-line system, located in the high-pressure laboratory and accessible at any time, is very useful for checking the sample loading. An on-line system, located in the experimental hutch, is used to control the pressure in the cavity of the cell mounted on the goniometer without unloading at each pressure step.

The optical system of the on-line device is placed on the X-ray axis behind the cell and can be remotely moved off the beam when the measurement is completed (Fig. 1). The same system, coupled to a CCD camera, is also used to image the cavity on a TV monitor.

2.1.6. *Choice of X-ray wavelength*. The wavelength selected in these experiments was $\lambda = 0.3738$ Å (corresponding to the iodine K-absorption edge at 37.169 keV; $2\theta_{max}$ at 1.5 Å resolution = 14.31°), which is popular at ID30. If the MAR345 detector is still used during forthcoming experiments, we plan to use a different wavelength on the basis of the following considerations. The sensitive layer of the imaging plate is made of BaFBr:Eu^{2+}; for 30–45 keV photons, the DQE depends essentially on the absorption coefficient of barium. This coefficient is largest at the 'peak' wavelength close to the Ba K-absorption edge ($\lambda = 0.3311$ Å, $E = 37.441$ keV; $2\theta_{max}$ at 1.5 Å resolution = 12.67°). Further, at this wavelength, the DQE is lower for photons inelastically scattered by diamonds than it is for photons elastically scattered by the sample. From standard formulae, the energy shift of Compton scattering is given by δE (eV) = $h^2/(2med^2)$ where h, m and e are Planck's constant and mass and charge of an electron, respectively, and $d = \lambda/(2\sin\theta)$ is the crystallographic resolution. Although small at low resolution (6 eV at 5 Å resolution), this shift is sufficient at medium (16.7 eV at 3 Å resolution) and high resolution (66.8 eV at 1.5 Å resolution) to produce a significant variation of the barium absorption coefficient, hence of DQE. This effect will thus improve the signal-to-background ratio where most useful, *i.e.* in the region of the diffraction pattern where signals are weakest.

2.2. *Sample mounting and alignment*

Disc-shaped gaskets cut in a stainless steel sheet (thickness 250 μm) were used. After indenting the gasket by appropriate squeezing, a cylindrical cavity (diameter 250 μm, thickness 150–170 μm) is machined using an automatic spark eroder (from Betsa). In one case, the cavity was eroded to obtain a near-elliptical cross section, which allowed to host an elongated SOD crystal. After ultrasonic cleaning, the gasket is remounted on the anvil in the initial position, the cell is closed by screwing the cap (Fig. 2) and a moderate pressure is applied again. Then, the cell is open and is now ready for loading. A crystal is fished in the crystallization drop using a nylon loop (from Hampton), then quickly transferred to a small drop (3–4 μl) of mother liquor covering the indentation. The drop must be deposited just before the deposition of the crystal, in order to reduce evaporation of its most volatile components. Then the crystal is gently pushed into the cavity. At this step, the behavior of the crystal depends on the composition of the liquor. In the case of tHEWL crystals, grown in a solution with a high concentration of NaCl, the sample tends to attach spontaneously to the cavity wall, whereas in the case of SOD grown in a solution with poly(ethylene) glycol, the crystal floats and its introduction into the cavity is more difficult. A tiny spherical ruby chip is deposited at the centre of the piston anvil. Then, the piston anvil is remounted and the cell is closed. A moderate pressure on the membrane seals the cavity, with the ruby chip near the axis of the cavity.

The cell is attached on the χ-cradle of the goniometer set at $\omega = 0$. The centre of the cavity must be accurately located on both the goniometer rotation axis and the X-ray beam pathway. This is realised in two steps. First, the cell is scanned along the y direction (*i.e.* perpendicular to the beam in the horizontal plane) at $\pm\omega$-angles. The intensity transmitted through the cavity is monitored by the photodiode. The centre of the cavity is on the rotation axis when the transmitted signals at $\pm\omega$ are equal. Second, the centre of the cavity is placed on the X-ray beam by scanning along z (the vertical direction). When this alignment is completed, the optical system (which allows to visualize the cavity, the crystal and the ruby chip on a TV monitor) is switched on. The X-ray beam position (at the centre of the cavity) is marked by a dot on the TV monitor. Then, it is easy to bring a fresh (*i.e.* non-irradiated) region of the crystal into the X-ray beam by step translations along the y and z directions. Irradiating successively different regions of the sample during data collection was an efficient way of alleviating the relatively fast degradation of crystals irradiated at room temperature.

3. Experiments on tHEWL crystals

HEWL was the first protein selected for our experiments, as it is the macromolecule which has been most thoroughly studied under high pressure and can be easily crystallized. According to experimental conditions, several crystalline forms can be obtained. The polymorph with the highest symmetry, tHEWL (space group $P4_32_12$), is the obvious choice with respect to geometrical limitations of the pressure cell. The ideal orientation for a tHEWL crystal is with c^* parallel to the rotation axis, for which the angular range is the smallest. Some observations on the stability of tHEWL crystals under high pressure have been reported. Crystals grown at atmospheric pressure in 0.83 M NaCl crack when being pressurized between 0.03 and 0.04 GPa, but can be brought to at least 0.1 GPa if the salt concentration is raised to 1.4 M before pressurization (Kundrot & Richards, 1987). This finding may be possibly explained by the variation of solubility of the protein as a function of pressure and the dependence of this variation with salt concentration. Indeed, pressure enhances solubility, but the slope of the variation is reduced by increasing salt concentration (Gross & Jaenicke, 1991). Katrusiak & Dauter (1996) have reported that the diffraction pattern of tHEWL crystals disappears at pressures which can be, on some samples, as low as 0.15 GPa,

Table 1
Unit-cell parameters and unit-cell volume of tHEWL crystals *versus* pressure.

Values noted with an asterisk (*) in the crystal column correspond to data sets from which integrated intensities have been measured.

Pressure (GPa)	$a = b$ (nm)	c (nm)	V (nm^3)	Crystal
0.0001	7.9223	3.7992	238.45	1
0.0001	7.9462	3.7799	238.67	2(*)
0.051	7.9009	3.8047	237.51	1
0.110	7.8695	3.8091	235.89	1
0.160	7.8511	3.8082	234.74	1
0.215	7.8216	3.8090	233.02	1
0.277	7.7925	3.8060	231.11	1
0.300	7.7788	3.8336	231.97	2(*)
0.300	7.7919	3.8069	231.13	4(*)
0.300	7.7666	3.8133	230.02	5
0.350	7.7861	3.7957	230.11	3(*)
0.368	7.7665	3.8073	229.65	1
0.403	7.7543	3.8062	228.86	1
0.481	7.7218	3.8003	226.60	1
0.500	7.7028	3.8001	225.47	5
0.568	7.6972	3.7947	224.82	1
0.580	7.6991	3.7822	224.19	3(*)
0.580	7.6956	3.7900	224.45	4(*)
0.600	7.6781	3.7935	223.64	5
0.645	7.6755	3.7894	223.25	1
0.670	7.6633	3.7886	222.49	5
0.690	7.6612	3.7721	221.40	3(*)
0.690	7.6626	3.7802	221.96	4(*)
0.690	7.6590	3.7864	222.11	5
0.725	7.6498	3.7863	221.57	5
0.750	7.6435	3.7837	221.06	5
0.770	7.6388	3.7816	220.66	5
0.800	7.6327	3.7791	220.16	5
0.820	7.6259	3.7754	219.56	5
0.880	7.6180	3.7543	217.88	5
0.915	7.5963	3.7053	213.81	5

but the crystallization conditions of these (in particular the salt concentration) were not specified.

HEWL (from Boehringer) was used without further purification to prepare tetragonal crystals. Using the hanging-drop vapor-diffusion technique, crystals were grown in solutions containing 50 m*M* sodium acetate buffer pH = 4.5 and 1.0–1.9 *M* NaCl with a protein concentration of 40 mg ml^{-1}. Crystals grown with 1.7 *M* NaCl turned out to be of ideal quality and shape and were finally retained for two distinct experiments at ID30.

A preliminary 15 h experiment with a low-intensity beam (single-bunch mode) allowed us to assemble the various pieces of equipment, establish the technique for loading a crystal in the pressure cell and collect and analyze high-quality oscillation images. The net result was the determination of the compressibility of tHEWL up to 0.645 GPa. The main experiment was performed over five days with a medium-intensity beam (16-bunch mode). Most of the allocated beam time was used to collect diffraction data from tHEWL crystals at several pressures, and the rest for experiments on SOD crystals. A fast analysis of most images was performed on-line during this experiment, in order to control and refine the experimental procedure.

3.1. *Preliminary experiment*

During cell loading, the relatively rapid evaporation of water in the drop deposited at the surface of the gasket tends to increase the salt concentration. Accordingly, the NaCl concentration of the solution deposited on the gasket cavity was lower than the NaCl concentration of the mother liquor. A crystal (crystal 1 in Table 1) was transferred into a 0.8 *M* NaCl solution. The sample and a ruby chip within the cavity are shown in Fig. 3. The pressure was gradually increased to 0.645 GPa, then the pressure increased too rapidly from 0.645 to 0.800 GPa which led immediately to the almost complete disappearance of the diffraction pattern. During the pressure ramp, single oscillation images (oscillation range 0.5°) were recorded at 11 pressures ranging from atmospheric pressure to 0.645 GPa. On visual inspection, these images looked extremely promising. They were devoid of powder rings from the gasket or cell material. Bragg spots from diamonds were scarce and easily discriminated from the tiny spots of the sample diffraction pattern. Background, owing mainly to elastic and inelastic scattering from diamonds, was quite uniform. The program *DENZO* (Otwinowski & Minor, 1997) was used to process the images, which were interpreted individually. Autoindexation led unambiguously to a primitive tetragonal lattice. The X-ray wavelength (0.3738 Å) and the crystal-to-detector distance (fixed to 700.00 ± 0.05 mm using calibration with the silicon standard) were kept constant; unit-cell parameters, three crystal orientation angles, coordinates of the direct beam and scanner distortion parameters were refined by least-squares fit of predicted and observed positions and partialities of all reflections. Absolute values of unit-cell dimensions obtained following this procedure, as well as the relative differences between measurements at different pressures, are quite accurate. Indeed, the main uncertainty is on the actual value of the pressure since an increase of 0.02 GPa has been observed several times between the initial pressure setting up preceding diffraction data collection and the final pressure check after data collection.

During this preliminary experiment, which was performed with a low-intensity beam and a relatively short cumulated exposure to X-rays, the crystal degradation was negligible.

3.2. *Main experiment*

During this experiment, the storage ring was operated in the 16-bunch mode, with an average intensity of about 70 mA. Three crystals (crystal 2 to crystal 4 in Table 1) transferred into a 1.0 *M* NaCl solution were used to collect diffraction data at different pressures. The crystal-to-detector distance was set to 600.00 ± 0.05 mm. The oscillation range and the exposure time per image were 0.75° and 60–120 s, respectively. A typical diffraction image is reproduced in Fig. 4. The total oscillation range was 42° (±21° around $\omega = 0$). During data collection with these crystals, which was performed with a medium-intensity X-ray beam and a long cumulated exposure, a continuous decrease of the resolution was observed. To alleviate this problem, as mentioned previously, the crystal was displaced by 50 µm every 20 images (Fig. 5). The number of collected diffraction images was up to

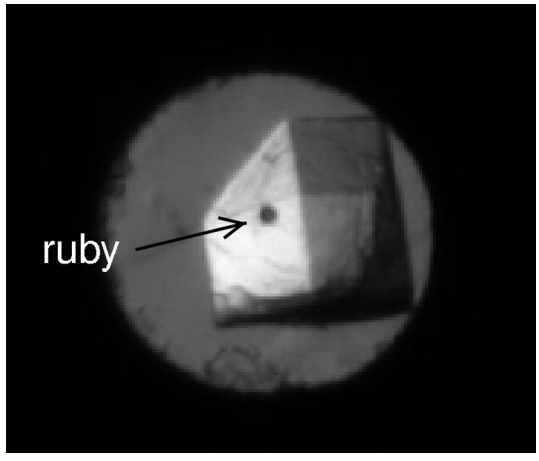

Figure 3
tHEWL crystal loaded in the pressure cell with a ruby chip.

Table 2
Summary of processing of individual data sets.

Values in parentheses refer to the corresponding values in the highest-resolution shell.

Pressure (GPa)	Crystal	Number of images	Resolution (Å)	R_{sym} (%)	Completeness (%)	Multiplicity
10^{-4}	2	46	2.24	8.4 (27.9)	55.7 (55.5)	4.5 (4.6)
0.300	2	58	2.00	6.2 (26.2)	67.9 (67.9)	4.0 (4.1)
0.300	4	57	2.12	6.5 (21.7)	89.7 (89.9)	3.1 (3.3)
0.350	3	54	1.90	5.1 (20.1)	63.5 (64.2)	4.2 (4.3)
0.580	3	54	2.12	7.9 (22.5)	61.2 (61.6)	4.3 (4.4)
0.580	4	56	2.27	9.7 (26.8)	88.1 (88.2)	3.1 (3.2)
0.690	3	39	2.58	9.1 (22.6)	64.8 (66.4)	2.8 (2.9)
0.690	4	12	2.10	7.2 (24.2)	55.7 (55.7)	1.2 (1.2)

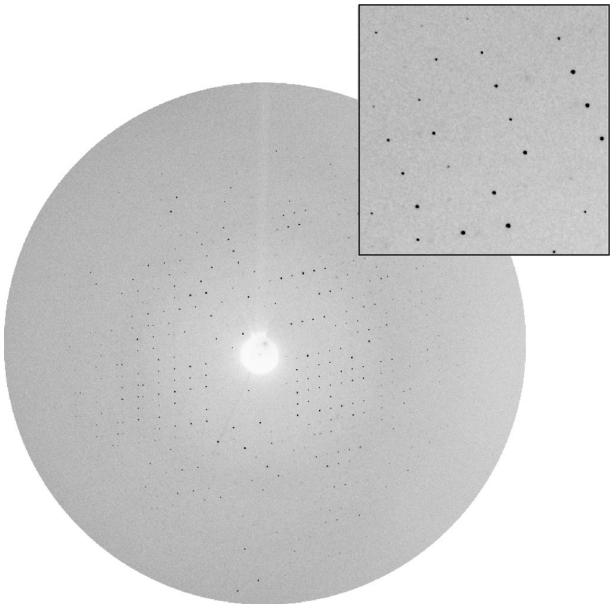

Figure 4
Typical diffraction picture obtained with a tHEWL crystal compressed at 0.35 GPa in the diamond cell. Conditions: unfocused undulator radiation, λ = 0.3738 Å, oscillation range 0.75°, exposure time 120 s at I = 70 mA, crystal-to-detector distance 600 mm, useful resolution 1.85 Å. A zoom of a portion of the picture is included.

about 60 for each crystal (20 images × 3 positions). Data were processed using *DENZO*. In the first as well as in the last images, a part of the diffraction pattern was obscured by anvil supports. Relevant reflections were eliminated from subsequent data processing. The program *SCALEPACK* was used to refine the crystal parameters. A unique set of cell parameters was refined for each data set. These cell parameters are reported in Table 1 and plotted *versus* pressure in Fig. 6. Since small crystal movements were observed during data collection, the three crystal orientation angles were refined for each image. Integrated data from a given data set were scaled together using the program *SCALA* from the *CCP*4 suite of programs (Collaborative Computational Program, Number 4, 1994). A summary of data processing of each individual data set is reported in Table 2. Data recorded at the same pressure on different crystals were merged together using *SCALA*. A summary of data-merging results is reported in Table 3.

The last crystal (crystal 5 in Table 1) was rapidly transferred into a drop with a higher salt concentration, 1.6 *M*, in order to complete measurements of cell parameters at the highest pressures. The same oscillation range of 0.75° was used to record an image at each pressure. The pressure was carefully ramped and high-quality diffraction was observed up to 0.82 GPa (Fig. 7*a*). At 0.88 GPa the crystal was damaged as evidenced by elongated and/or split Bragg reflections (Fig. 7*b*). Keeping the pressure constant, the same image was repeatedly recorded. The quality of the pattern restored after 10 min (Fig. 7*c*), becoming comparable with the quality observed at

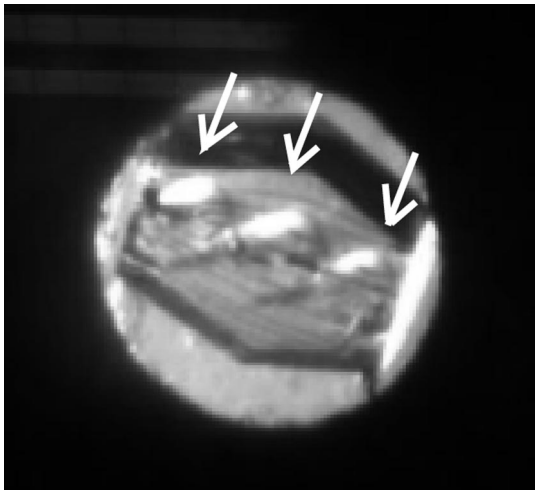

Figure 5
tHEWL crystal after long X-ray exposures at three different positions, showing clearly the degradation of irradiated regions marked with arrows.

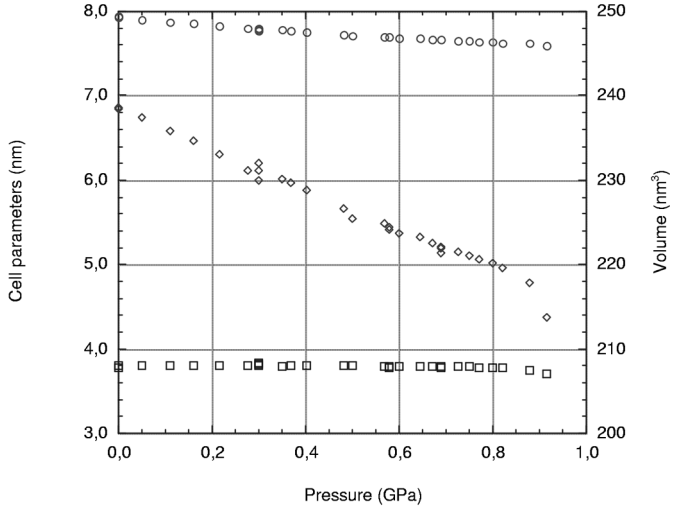

Figure 6
Variation of unit-cell parameters a (circles) and c (squares) and unit-cell volume (diamonds) of tHEWL crystals as a function of pressure at room temperature.

Table 3
Summary of merging between data sets taken at the same pressure on different crystals.

Values in paretheses refer to the corresponding values in the highest-resolution shell

Pressure (GPa)	Crystals	Resolution (Å)	R_{merge} (%)	Completeness (%)	Multiplicity
0.300	2, 4	2.09	8.5 (27.6)	91.0 (92.0)	6.0 (6.3)
0.580	3, 4	2.23	8.2 (24.0)	99.5 (99.7)	5.2 (5.3)
0.690	3, 4	1.90	7.5 (23.9)	75.7 (62.1)	4.4 (4.8)

0.82 GPa, but with a substantial contraction of unit-cell parameters, especially *c* (Table 1), producing a 1.9% relative variation of cell volume. Then, diffuse scattering began to appear between Bragg spots (Fig. 7*d*) 20 min later. Gradual transfer of intensity from the diffraction pattern to diffuse scattering was then observed, leading to disappearance of diffraction after 20 min. This vanishing was partly radiation-induced since the quality of the diffraction pattern from a fresh part of the crystal at 0.88 GPa (Fig. 7*e*) observed during a period of 10 min was again comparable with the quality observed at 0.82 GPa. The pressure was then set to 0.915 GPa and the diffraction pattern immediately showed evidence of diffuse scattering between Bragg spots (Fig. 7*f*). Finally, diffraction disappeared at this pressure after a period of 15 min.

4. Discussion

4.1. *Results on lysozyme*

The high-pressure crystal structure of tHEWL at room temperature and 0.1 GPa has been reported by Kundrot & Richards (1987, 1988). The unit-cell volume contracted by about 1.1% between ambient pressure and 0.1 GPa. The detailed analysis of the three-dimensional structure demonstrated the unique interest of crystallography to image local pressure-induced changes in a protein molecule. The high-pressure beryllium cell (Kundrot & Richards, 1986) had limitations in that optical observation was not possible and the range of pressure was limited (maximum design pressure: 0.2 GPa). Experiments were performed without area detector and using Cu $K\alpha$ radiation which was strongly absorbed by the cell walls. Katrusiak & Dauter (1996) have used a commercial Merrill–Bassett (Merrill & Bassett, 1974) diamond-anvil cell, an imaging-plate detector and synchrotron radiation from a bending magnet for compressibility measurements on both tHEWL and oHEWL (orthorhombic polymorph) crystals. The oHEWL crystal could be compressed to beyond 1 GPa; the volume compressibility was 0.17 GPa^{-1} between 0.1 and 0.4 GPa and 0.15 GPa^{-1} to 1 GPa. The diffraction of tHEWL crystals disappeared at about 0.2 GPa, and even at 0.15 GPa in one case.

Our results on tHEWL confirm that protein crystals can be hydrostatically compressed to high pressures. Excellent crystalline order can be preserved if pressure is ramped slowly and continuously. Using crystals grown and maintained in high salt concentration, tHEWL crystals could be compressed to a much higher pressure than reported by Katrusiak & Dauter (1996). The variations of cell parameters and cell volume of tHEWL as a function of pressure are shown in Table 1. The compression is anisotropic; the *c* axis is almost constant while the *a* axis contracts. The compressibility is approximately linear (average value: $\chi = 0.098\ GPa^{-1}$). In fact, the compressibility decreases as pressure increases and, with respect to linear regression, a better agreement is obtained by fitting the experimental data with a polynomial of degree 2. Results of Kundrot & Richards (1987) are confirmed and extended to much higher pressures. The compressibility of tHEWL is about two-thirds of the compressibility of oHEWL (Katrusiak & Dauter, 1996) and, as pointed out by these authors, is comparable with the compressibility of much harder hydrogen-bonded molecular crystals. For instance, the compressibility of 2-methyl-1,3-cyclohexanedione is 0.096 GPa^{-1} (Katrusiak, 1991). Diffraction data sets have been collected and processed for several tHEWL crystals at different pressures. Best results for individual processing of data sets (Table 2) were obtained for crystal 3 at 0.350 GPa (resolution 1.9 Å, redundancy 4.2, R_{sym} = 0.051; absorption correction would improve R_{sym} by 0.01–0.02). The completeness was limited to 63.5% due to geometrical limitations of the pressure cell. Data sets from individual crystals recorded at the same pressure (0.69, 0.58 and 0.30 GPa, respectively) have been merged. Merged data sets at 0.58 and 0.30 GPa are essentially complete. The merged data set at 0.69 GPa is of good quality, but the completeness is lower. The three structures were refined using the *SHELXL* program (Sheldrick, 1997) at the nominal resolution of the measured data. The final statistics are given in Table 4. A detailed structural analysis will be published in a separate article.

From these data, one can obtain estimates of the compressibility of selected portions of the molecule and of those portions of solvent that

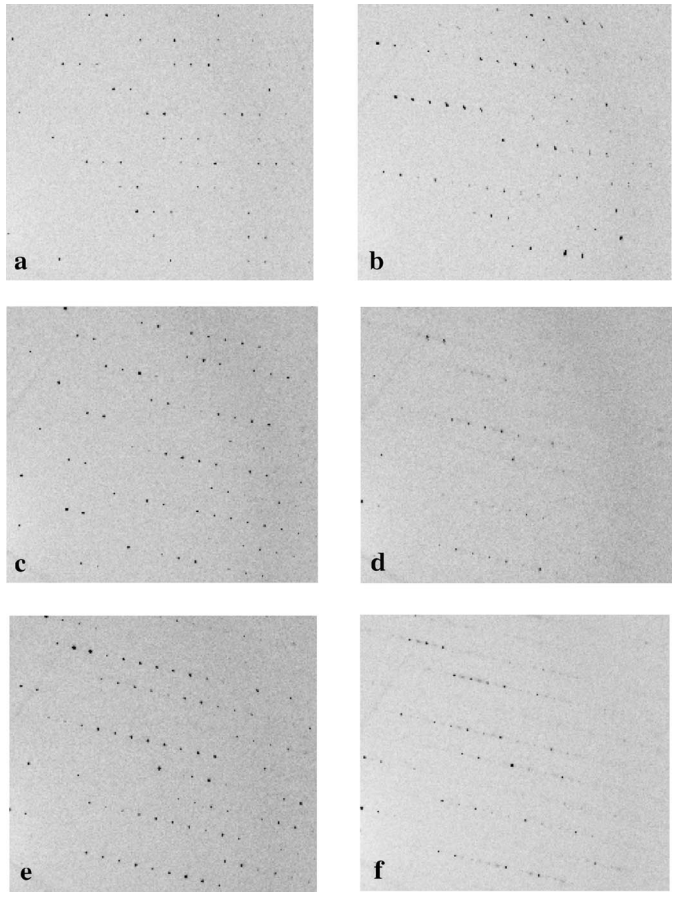

Figure 7
Course of pressure-induced loss of crystalline order in a tHEWL crystal, followed by multiple recording of the same frame. (*a*) At 0.82 GPa. (*b*) Immediately after ramping at 0.88 GPa. (*c*) Restoration of crystalline order after 10 min at 0.88 GPa. (*d*) Onset of diffuse scattering at 0.88 GPa. (*e*) Diffraction from a fresh crystal part at 0.88 GPa. (*f*) Onset of diffuse scattering immediately after ramping at 0.915 GPa.

Table 4
HEWL structures at 0.30, 0.58 and 0.69 GPa.

Statistics after refinement.

	Pressure (GPa)		
	0.3	0.58	0.69
Parameters used			
$a = b$ (Å)	77.54	76.77	76.58
c (Å)	38.05	37.87	37.85
Refinements			
Resolution limits (Å)	18–1.98	18–1.99	18–1.81
R-factor (%) for observed reflections [$F \geq 4\ \sigma(F)$]	18.5	20.6	21.5
R-factor (%) for all reflections	21.8	23.1	25.5
No. of reflections used (observed/all)	6390/7666	6564/8072	6266/8093
No. of parameters/No. of restraints	4209/4255	4177/4272	4141/4278
RMS deviations from ideality			
1–2 (covalent) bond lengths (Å)	0.007	0.006	0.006
1–3 (angle) bond lengths (Å)	0.019	0.020	0.020
Zero-chiral volumes (Å^3)	0.079	0.081	0.081
Non-zero chiral volumes (Å^3)	0.085	0.086	0.090
Planes (Å)	0.107	0.108	0.110
Density residuals in last ($F_o - F_c$) map (e$^-$)	+0.24/−0.26	+0.29/−0.25	+0.30/−0.38

can be reliably identified in electron density maps, and probe changes in ordered water molecules and bonding between them as well as between water molecules and protein molecules.

Another interesting question is what single-crystal X-ray diffraction can tell us about the global and local onset of pressure-induced denaturation. Pertinent information on this subject may be derived from overall and detailed features of both diffraction and diffuse scattering patterns, as well as from atomic temperature factors and electron densities of various parts of the protein molecule at different pressures. At 0.88 GPa and beyond, we have observed an abnormal behaviour of the crystal that is probably due to pressure-induced denaturation of protein molecules in the crystal. The loss of crystalline order deserves a more detailed investigation based on the acquisition of complete data sets and not only single images.

Finally, our results confirm that proteins may be more resistant to denaturation in crystals than in solution (Heremans & Wong, 1985; Chen & Heremans, 1990). The preservation of crystalline order in tHEWL shows that denaturation of protein molecules remains limited up to at least 0.82 GPa. In solution, the pressure denaturation of lysozyme probed by ultraviolet fluorescence occurs at lower pressures (Li *et al.*, 1976). Observations involved both measurements of the intrinsic fluorescence spectrum and fluorescence yield of lysozyme and characterization of a ligand-protein equilibrium by measurements of the fluorescence of ANS, a hydrophobic ligand that binds unfolded proteins. Fluorescence enhancement of ANS in the presence of lysozyme reveals that protein denaturation occurs above 0.6 GPa, while decrease of the fluorescence yield of the enzyme is conspicuous at much lower pressures.

4.2. *Improvements in material and methods*

Various improvements will be made in future HPPX experiments on the ID30 beamline:

(i) A correction for the absorption of X-rays by diamonds will be implemented, based on the calculation of pathway lengths of incoming and diffracted beams across diamonds for each Bragg reflection.

(ii) A new design of the pressure cells will increase optical apertures to about 60°, which is possible as the useful range of pressure is limited to about 2 GPa.

(iii) The signal-to-noise ratio (*i.e.* the ratio of diffraction signal to background on diffraction images) will be improved. As previously discussed, the X-ray wavelength should be selected to maximize the detector DQE for elastical scattering while reducing the efficiency for inelastic scattering. In the case of an imaging plate, the optimum wavelength is very close to the Ba K edge. In the case of a CCD detector, the wavelength should be selected according to the elemental composition of phosphor. Further, the short CCD dead time will allow the use of smaller oscillations, thus contributing to reduce background.

(iv) In the normal mode of operation of the ESRF (two-thirds filling), the exposure time per frame will be twice as short with respect to the 16-bunch mode used during these experiments. Data collection rate will be further increased by using a CCD detector with a short dead time instead of the imaging-plate scanner.

4.3. *Potential applications of HPPX*

A crystal is a sample in a uniquely well defined and homogeneous state that can be reproduced at will by using definite conditions to grow crystals. For the two proteins that we have selected for these first experiments, good crystals could be preserved over a wide range of pressure. Further, it was demonstrated that high-quality data can be collected with the present equipment on ID30. As discussed above, the resolution that has been achieved, although respectable, can be improved, and this will be a major concern for future experiments. Accordingly, the prospect is the determination of accurate structural parameters in a broad range of pressure. Such data were scarce up to now, and their availability for a number of proteins will have many applications:

(i) Reliable structural parameters are necessary for determining and refining parameters for structure-based calculations of important thermodynamic quantities such as the enthalpy change in protein folding and binding. Recent results rationalize the observation that the enthalpy change of protein folding/unfolding scales in terms of changes in accessible surface areas, and provide a way to incorporate explicitly the effects of packing density in the structure-based prediction of enthalpy changes (Hilser *et al.*, 1996). A first set of parameters has been derived with the structural data at hand. While this parameterization predicts protein unfolding enthalpies with an error close to 3%, the values of the parameters will be refined as more data, covering situations in which specific interactions can be better defined, become available.

(ii) The investigation of interactions is another broad field where accurate structural parameters are crucial. This includes: (*a*) interactions between protein molecules, including the effect of salts on structure stability and understanding why proteins may be more resistant to denaturation in the crystal than in solution; (*b*) structural principles of organization of oligomeric proteins, which are complex assemblies which may be dissociated by even relatively modest pressures (0.2 GPa or less) weakening electrostatic and hydrophobic contacts which stabilize quaternary structure.

(iii) The study of pressure-induced denaturation in the crystalline state is essentially an open field. In contrast to NMR and spectroscopic techniques, the constraint of long range order limits the amplitude of atomic displacements/motions, and it can be anticipated that denaturation will take place fairly suddenly in a narrow pressure range, as seen in the case of tHEWL crystal 5. A technical problem, at least with monochromatic X-ray radiation, might be the time required to collect a fairly complete data set for a fast-evolving state.

5. Conclusions

Undulators inserted in a high-energy electron storage ring, such as at the ESRF, and emitting intense and near-parallel X-rays of ultra-short wavelength are a breakthrough for HPPX. The combination of such undulators with a diamond-anvil cell and a large area detector with good DQE opens new prospects for accurate structural studies of macromolecules under high pressure.

The staff on ID30 at the ESRF are gratefully acknowledged. We thank Madalena Renouard for her collaboration to crystal growth at LURE, and Jean Vicat for his collaboration to crystal mounting at the ESRF.

References

Ascone, I., Fourme, R., Kahn, R., Mézouar, M., Hoerentrup, C. & Renouard, M. (2001). In preparation.
Chen, G. & Heremans, K. (1990). *High Press. Res.* **5**, 749–751.
Chervin, J. C., Canny, B., Besson, J. M. & Pruzan, P. (1995). *Rev. Sci. Instrum.* **66**(3), 2595–2598.
Collaborative Computational Program, Number 4 (1994). *Acta Cryst.* D**50**, 760–763.
Ekstrom, J. L., Ealick, S. E., Osterberg, F. H. O. & Gruner, S. (1995). Am. Crystallogr. Assoc. Meet., Montreal, Canada. Abstract A319.
Fourme, R. (1968). *J. Appl. Cryst.* **1**, 23–30.
Gross, M. & Jaenicke, R. (1991). *Eur. J. Biochem.* **221**, 617–630.
Jonas, J. & Jonas, A. (1994). *Ann. Rev. Biophys. Biomol. Struct.* **23**, 287–318.
Heremans, K. & Wong, P. T. T. (1985). *Chem. Phys. Lett.* **118**, 101–104.
Hilser, V. J., Gomez, J. & Freire, E. (1996). *Proteins*, **26**(2), 123–133.
Katrusiak, A. (1991). *High Press. Res.* **6**, 155–167.
Katrusiak, A. & Dauter, Z. (1996). *Acta Cryst.* D**52**, 607–608.
Kriechbaum, M., Steinhart, M., Pressel, K. & Laggner, P. (1994). *23rd Steenbock Symposium on High-pressure Effects in Molecular Biophysics and Enzymology*. University of Wisconsin, Madison, USA.
Kundrot, C. E. & Richards, F. M. (1986). *J. Appl. Cryst.* **19**, 208–213.
Kundrot, C. E. & Richards, F. M. (1987). *J. Mol. Biol.* **193**, 157–170.
Kundrot, C. E. & Richards, F. M. (1988). *J. Mol. Biol.* **200**, 401–410.
Le Toullec, R., Pinceaux, J. P. & Loubeyre, P. (1988). *High Press. Res.* **1**, 77–90.
Li, T. M., Hook, J. W., Drickamer, H. G. & Weber, W. (1976). *Biochemistry*, **15**(25), 5571–5580.
Mao, H. K., Bell, P. M., Shaner, J. W. & Steinberg, D. (1978). *J. Appl. Phys.* **49**, 3276.
Merrill, L. & Bassett, W. A. (1974). *Rev. Sci. Instrum.* **45**, 290–294.
Mozhaev, V. V., Heremans, K., Frank, J., Masson, P. & Balny, C. (1996). *Proteins*, **24**, 81–91.
Otwinowski, Z. & Minor, W. (1997). *Methods Enzymol.* **276**, 307–326.
Sheldrick, G. (1997). *SHELX97. Program for Refinement of Crystal Structures.* University of Göttingen, Germany.
Silva, J. L. & Weber, G. (1993). *Ann. Rev. Phys. Chem.* **44**, 89–113.
Urayama, P. (1999). IUCR Meeting, Glasgow, UK. Abstract M11.0c.005.
Van Valkenburg, A. (1962). *High Pressure Measurements*, edited by A. A. Giardiniand & E. C. Lloyd, p. 87. Washington: Butterworths.

 Received 9 March 2001 • Accepted 28 June 2001